European Journal of Pharmaceutical Sciences 47 (2012) 965–978

Contents lists available at SciVerse ScienceDirect

European Journal of Pharmaceutical Sciences

journal homepage: www.elsevier.com/locate/ejps

Intestinal permeability of lamivudine (3TC) and two novel 3TC prodrugs. Experimental and theoretical analyses

María S. Gualdesi, Margarita C. Briñón, Mario A. Quevedo *

Departamento de Farmacia, Facultad de Ciencias Químicas, Universidad Nacional de Córdoba, Haya de la Torre esq., Medina Allende s/n, Ciudad Universitaria, 5000 Córdoba, Argentina

ARTICLE INFO

Article history:
Received 26 July 2012
Received in revised form 3 October 2012
Accepted 4 October 2012
Available online 13 October 2012

Keywords:
Lamivudine
Intestinal absorption
Prodrugs
P-glycoprotein
Molecular modeling

ABSTRACT

Lamivudine (3TC) is an antiviral drug with a widely demonstrated clinical efficacy used to treat Acquired Immunodeficiency Syndrome (AIDS) in humans. However, since the rapid emergence of resistant viral strains has limited its effect, several new strategies such as the design of prodrugs have been applied to try to optimize its pharmacotherapeutic properties. The present study deals with the intestinal permeation of 3TC and two novel prodrugs of 3TC, namely 3TC-Etha and 3TC-Buta, by using rat intestinal segments and applying the gut sac *in vitro* technique. An adequate bioanalytical method (sample preparation and quantitative analysis) was fully developed and validated for the quantitation of these three compounds. A low permeability coefficient (P_{app} 0.408 ± 0.049 × 10^{-4} cm/min) was found for 3TC if compared to that previously reported for zidovudine (2.38 ± 0.12 × 10^{-4} cm/min), while no statistically significant differences were observed in its apical-to-basal or basal-to-apical permeabilities. Our data suggests that 3TC permeates through the intestinal tissue by passive diffusion, with no intervention of efflux mechanism during this process as determined applying the gut sac technique. Regarding the prodrugs, both 3TC-Etha and 3TC-Buta were able to increase 3TC permeability (2 and 10 times, respectively), but none of these compounds were capable of crossing the intestinal tissue in their intact forms. In the case of 3TC-Etha, the permeability of the intact compound (P_{app} 0.093 ± 0.010 × 10^{-4} cm/min) was impaired by a P-glycoprotein (P-gp) mediated efflux, evidenced by the higher permeability coefficient (6.933 ± 0.586 × 10^{-4} cm/min) determined in the presence of verapamil on the apical side of the enterocyte. In contrast, 3TC-Buta was not subjected to efflux mechanisms on the apical side of the enterocyte, but was efficiently converted to 3TC by enzymatic hydrolysis during the permeation process. In the light of these results, molecular modeling (docking and molecular dynamics) techniques were applied to study further the structural features that may confer the different behaviors of these two compounds with respect to P-gp mediated efflux. The results also highlight the potential of combining experimental and theoretical studies in the design of 3TC prodrugs with enhanced intestinal permeation properties.

1. Introduction

As a result of the continuous progression of the Acquired Immunodeficiency Syndrome (AIDS) in the world, intensive efforts are currently being made to develop new compounds capable of inhibiting the replication of type-1 human immunodeficiency virus (HIV-1) (Esté and Cihlar, 2010). Significant advances have already been obtained in the pharmacotherapy of AIDS, with the disease being transformed from an "inherently untreatable" pathologic condition to a chronically manageable one (Samuel, 2010). Many of these achievements are related to the availability of a wide range of anti-HIV-1 drugs, thereby further developing the Highly Active Antiretroviral Therapy (HAART) schemes (Andrew, 2010; Esté and Cihlar, 2010). Among these drugs, the nucleoside reverse transcriptase inhibitors (NRTI's) represent the first and most widely studied family of compounds, with their effectiveness in inhibiting the viral replication having being extensively demonstrated (Cihlar and Ray, 2010). Unfortunately, none of these compounds is devoid of clinically relevant adverse effects, which sometimes limits the continuity of the antiretroviral treatment (Trevor, 2010). To date, nine NRTI's have been approved for clinical use, among which lamivudine (3TC, Fig. 1a) is a widely used agent, either alone or in combination with other antiretroviral compounds as part of HAART. Of these, 3TC is the only NRTI that has also been licensed for the treatment of infection by hepatitis B virus (HBV), a fact that has spread interest in this compound and its pharmacotherapeutic properties beyond anti-HIV-1 therapy. Although 3TC is one of the safest compounds among the NRTIs, it efficacy is limited by the rapid development of both HIV and HBV resistant strains (Gao et al., 2000). In an attempt to optimize

* Corresponding author. Tel.: +54 0351 4334163/4334127; fax: +54 0351 4334127.
E-mail address: alfredoq@fcq.unc.edu.ar (M.A. Quevedo).

0928-0987/$ - see front matter © 2012 Elsevier B.V. All rights reserved.
http://dx.doi.org/10.1016/j.ejps.2012.10.002

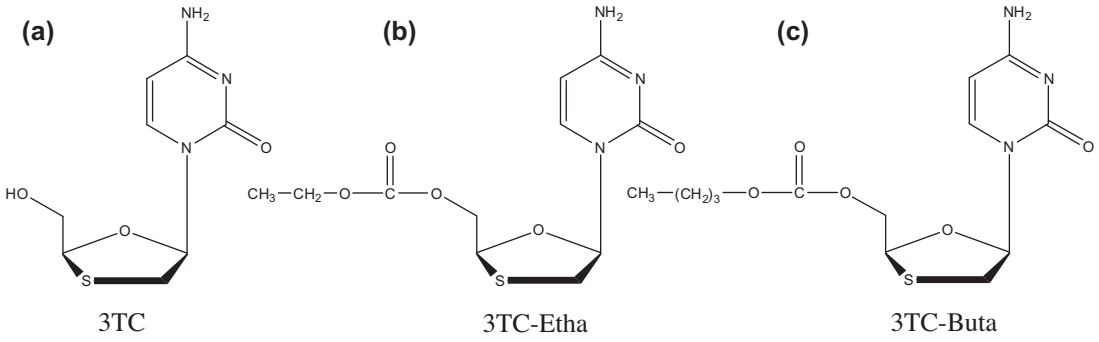

Fig. 1. Chemical structure of the compounds studied in this work.

its pharmacotherapeutic properties, several strategies have been envisioned, among which, the obtention of prodrugs has been widely applied. Consequently, the formation of 5-OH esters, carbonate and carbamate derivatives of 3TC has been explored in the search of compounds exhibiting a wide pattern of physicochemical properties and reconversion rates (Anastasi et al., 2003; Chimalakonda et al., 2007; Zhong et al., 2012).

In line with this efforts, the design of novel 3TC prodrugs was pursued by our research group by combining 3TC with several aliphatic alcohols through a carbonate linker function (Ravetti et al., 2009). After the biological activity was determined, most of these compounds retained anti-HIV-1 and anti-HBV activity *in vitro* (Gagey et al., 2010; Ravetti et al., 2009), and thus to continue their preclinical development, relevant physiochemical properties were studied, among which lipophilicity is of special interest due to the requirement of permeation through biological membranes (Ravetti et al., 2008). Although the results obtained to date suggest that these compounds may be interesting for further development, no information regarding their potential to permeate through the intestinal tissue after an oral dose has been obtained yet while literature dealing with 3TC intestinal permeability is scarce and somewhat variable (Mariappan and Singh, 2007; Strauch et al., 2011). A general consensus has now been reached that this drug may be classified in the Biopharmaceutical Classification System (BCS) as a class III compound (high solubility and low permeability) (Strauch et al., 2011). In this context, the present study deals not only with investigating the intestinal permeation of 3TC in the rat jejunum, but also with that of two novel lipophilic prodrugs of 3TC, namely 3TC-Etha and 3TC-buta (Fig. 1b and c). These prodrugs were selected among the compounds reported by Ravetti et al., since they exhibited a high combined potency, both in anti-HIV-1 and anti-HBV *in vitro* assays (Gagey et al., 2010; Ravetti et al., 2009).

2. Experimental

2.1. Chemicals and reagents

The drug 3TC and the internal standard (IS) AZT were generously provided by Filaxis (Buenos Aires, Argentina), while verapamil (VER) and quercetin (QUE) were purchased from Sigma–Aldrich Co. Carbonates 3TC-Etha and 3TC-Buta were synthesized following previously reported procedures (Ravetti et al., 2009). The Krebs–Ringer buffer (KRB) (6.94 mg/ml NaCl; 0.35 mg/ml KCl; 0.27 mg/ml $CaCl_2$; 0.32 mg/ml $MgSO_4$; 0.37 mg/ml KH_2PO_4; 2.02 mg/ml $NaHCO_3$; 2.00 mg/ml Glucose) was prepared on the day of use in milli-Q water using *p.a.* reagents. Phosphate buffer (pH 7.4; 25 mM) was also freshly prepared using *p.a.* reagents. The HPLC grade methanol ($MEOH_{HPLC}$) used in chromatographic procedures was purchased from Sintorgan Co., with stock solutions and mobile phases being filtered through Millipore type FH filters (4.5 μm) and degassed under vacuum.

2.2. Apparatus

The HPLC analysis was carried out in an Agilent Technologies Series 1100 apparatus equipped with an autosampler module, thermostatic column compartments and a UV–Vis multiple wavelength (MWD) detector ($\lambda = 272$ nm). Instrumental control and chromatographic data acquisition were performed using the Agilent ChemStation (Rev. B.03.01) software. A Huber Polystat CC1 bath (±0.1 °C) was used for assays requiring temperature control, while a Crison GLP-21 equipped with a combined Ag/AgCl/glass electrode was used to measure the experimental pH of the solutions. Prior to performing quantitative analysis, samples were concentrated to dryness using a Techne Inc. sample concentrator coupled to an N_2 source.

2.3. Standard and stock solution preparation

Stock solutions of 3TC and its derivatives (0.150 mM), as well as the AZT (3.74 mM) used as internal standard, were prepared in $MeOH_{HPLC}$ prior to use. The stock solutions were diluted in KRB to obtain working standard solutions in the concentration range of 1.50×10^{-6} M to 1.12×10^{-4} M. The internal standard (20 μl) was added in all cases.

2.4. Sample preparation for 3TC, 3TC-Etha and 3TC-Buta quantification

In order to isolate the analytes from the KRB a solid phase extraction (SPE) protocol was developed and fully validated. Strata-X® (60 mg, Phenomenex®) SPE cartridges were used, and the following protocol was applied: (a) cartridges were preconditioned by sequentially applying 2.0 ml of $MEOH_{HPLC}$ which was followed (b) by an equilibration step of 2.0 ml of pH 7.4 (25 mM) phosphate buffer. The sample intended for extraction was prepared by adding the IS solution (20 μl, 1 mg/ml) to the corresponding sampled aliquots, which was homogenized and (c) was applied to the preconditioned cartridge at a flow rate of 1 drop/s. Prior to (d) elution with 1 ml of $MEOH_{HPLC}$, the cartridge was dried under vacuum for 1 min. Finally, (e) the eluate was concentrated under a N_2 stream at 40 °C and resuspended in 200 μl of mobile phase prior to HPLC analysis.

2.5. Quantitative (HPLC) analyses

Quantification was performed using the HPLC equipment described in the apparatus section. A Phenomenex Synergi Fusion®

C_{18} analytical column (4.0 × 250 mm, 5 μm particle size) and a Phenomenex Security Guard Fusion® RP (4.0 × 30 mm) guard column were used. The mobile phase consisted of a pH 7.4 phosphate buffer (25 mM): $MeOH_{HPLC}$: Tetrahydrofuran (THF) (60:38:2) mixture, with a flow rate of 1.1 ml/min. The analytical column was thermostated at 40 °C, injecting 10 μl of sample. Chromatograms were acquired and processed with the Agilent ChemStation (Rev. B.03.01) software, while statistical procedures were carried out using Microcal Origin v.8.0 software.

2.6. Chemical stability studies

Solutions of 3TC-Etha and 3TC-Buta (40 ml, 9.36×10^{-6} M) were prepared in KRB (5:95 CO_2:O_2) and incubated at 37 °C for 60 min. Aliquots (2 ml) were sampled at 10 min intervals, and subjected to the corresponding sample preparation and quantitative analysis procedure. The amounts of intact compound, as well as the 3TC regenerated in the incubation media, were determined from the corresponding concentration vs. time plots.

2.7. Animal treatments

Healthy male Wistar rats (250–300 g) were obtained from the bioterium of the Departamento de Química Biológica, Facultad de Ciencias Químicas, Universidad Nacional de Córdoba (FCQ-UNC), Argentina. All procedures involving the use of rats were reviewed and approved by the Committee of Ethics for the Use of Animals in Experimental Protocols of the FCQ-UNC, Argentina (Res. No. 138/07). Animals were caged with free access to water and food pellets until 24 h prior to performing the assays, after which, they were fasted and allowed to ingest water *ad libitum* until surgical procedures were carried out.

2.8. Intestinal permeation assays

The intestinal permeations of 3TC, 3TC-Etha and 3TC-Buta were studied by applying the intestinal gut sac technique (Quevedo and Briñón, 2009; Quevedo et al., 2011; Sharma et al., 2002). After rats were anesthetized by intraperitoneal administration of urethane (1000 mg/kg), a 2 cm incision was made in the midline abdominal cavity, isolating a segment of 10 cm of proximal jejunum (just 15 cm distal to the ligament of Treitz). After the tissues were dissected, rats were immediately sacrificed by applying CO_2. Intestinal segments were flushed with 30 ml of KRB (37 °C, 5% CO_2 and 95% O_2). In order to study the apical-to-basal (A/B) transport, the everted mode technique was applied by gently everting the intestinal segment on a glass rod. When the basal-to-apical (B/A) permeation direction was analyzed (non-everted mode), tissue segments were used immediately after being washed with KRB.

The device used for the permeation assay has been described in detail in a previous work (Quevedo and Briñón, 2009). Briefly, a glass cannula was inserted into the intestinal segment and tied at the top and bottom, with 10 cm of tissue being exposed to the drug permeation. Then, a 10 g weight was tied to the bottom of the segment, and the device with the tissue was submerged into 40 ml of warm pH 7.4, KRB (5:95 CO_2:O_2, 37 °C) containing the drug under study at the assayed concentration. The drug was added to the KRB dissolved in 50 μl of dimethyl sulfoxide. These conditions assured tissue viability during the whole assay sampling interval, a feature that was determined by means of the glucose concentration test as previously reported (Quevedo et al., 2011).

To perform the permeation assay, 1 ml of pH 7.4, KRB (5:95 CO_2:O_2, 37 °C) was placed into the intestinal segment and withdrawn at 10, 20, 30, 40, 50 and 60 min, and replaced by 1 ml of drug-free KRB. Between each permeation sample, 1 ml of pH 7.4 KRB (37 °C) was used to rinse the cannula, with this aliquot being added to the corresponding permeation sample. For procedures involving the inhibition of efflux transporters, KRB mucosal or serosal solutions containing VER (0.1 mM) and QUE (0.1 mM) were used. The collected aliquots were subjected to the described sample preparation technique (Section 2.4) and HPLC analysis protocol, with the corresponding results being subjected to the data analysis procedures shown below (Section 2.9). The permeation assays were performed in triplicate at each assayed concentration and experimental setup.

2.9. Data transformation and analyses

The cumulative quantity of drug vs. time was plotted, after which linear regression analyses were performed by calculating the corresponding coefficient of determination (R^2) to evaluate linearity. The flux (F, cm/min) through the intestinal tissue was determined from the corresponding linear fitting slope, while the apparent permeability coefficient (P_{app}) was calculated by applying Eqs. (1) and (2) (Balimane et al., 2000):

$$P_{app} = \frac{F}{Sup_{exp} Conc_{ini}} \quad (1)$$

$$Sup_{exp} = 2\pi rh \quad (2)$$

where Sup_{exp} is the surface available for permeation, $Conc_{ini}$ is the initial drug concentration in the donor solution, r is the intestinal segment mean radius (0.4 cm) and h is the length of intestinal segment available for permeation (10 cm). The corresponding *lag* permeation times were calculated from the intercept of the fitted equations obtained by linear regression analyses.

Results were expressed as the mean ± SD of three independent experiments. Comparisons between the calculated P_{app} values were performed by means of one-way analysis of variance (ANOVA) using the Microcal Origin v.8.0 software, while in the case of two data sets the Student's t-test was utilized. A p-value < 0.05 was considered as statistically significant.

2.10. Molecular modeling procedures

The initial structures of the molecules subjected to theoretical analyses (rhodamine-123, zidovudine, abacavir, 3TC, 3TC-Etha and 3TC-Buta) were constructed using the Gabedit software (Allouche, 2011), with further conformational and energetic optimization stages being performed using the Gaussian03 package. In this way, the minimum energy conformations of the ligands could be determined.

The complexes between the ligands and P-glycoprotein (P-gp) were predicted by a molecular docking approach based on the reported crystal structure of the proteins deposited in the Protein Databank (pdb: 3G60) (Aller et al., 2009). The molecular docking studies included the following protocol: (a) tautomer and ionization state analyses of the ligands; (b) conformer library generation; (c) docking pose prediction and (d) visualization and analysis of the results. (Stage a) was carried out by means of the *Moka v.1.1* and *MarvinSketch v.5.8.2* software packages (Milletti et al., 2007), with the ligand ionization states being assumed to be at pH 7.4. The ligand conformer libraries (stage b) were generated using the *Omega2 v.2.4.3* software (Hawkins et al., 2010), with conformers generated at an energy threshold of 10 kcal/mol. Prior to submitting the conformer libraries to the docking procedures, all conformers were assigned with AM1-BCC fitted charges. To perform the docking runs (stage c), the receptor molecule (P-gp) was prepared using the *Fred_Receptor v.2.25* software module, with a binding box volume of 6000 Å^3 centered on the binding cavity reported

for VER (Aller et al., 2009). The docking runs were performed with the *Fred v.2.2.5* software (McGann, 2011), and ranked using the *Chemgauss2* scoring function. The minimum energy binding pose was selected using the *Vida v.4.1.1* package, and further subjected to molecular dynamics analyses.

Molecular dynamics simulations were performed assuming an implicit solvent model using the *Amber12* software package (Case et al., 2005). Simulations were run based on the *ff03.r1* and *gaff* forcefields for the protein and ligands, respectively. Simulated systems were minimized for 20 picoseconds (ps), heated to 300 K for 50 ps before being simulated for 200 ps using a time step of 2 femtoseconds (fs), under constant pressure and temperature conditions (production phase). The SHAKE algorithm was applied to constrain bonds involving hydrogen atoms and since we were only interested in analyzing the recognition energetic behavior between the ligands and the *apo* form of P-gp, the protein backbone was restrained throughout the simulation. Trajectories and energetic component analyses were applied using the *ptraj* and molecular mechanics Poisson–Boltzmann surface area (MM-PBSA) modules of *Amber12* (Kuhn et al., 2005).

The corresponding structures were visualized using the *VMD v.1.8.6* software, and intermolecular interactions were detected and depicted with *Ligplot v. 1.3.6* (Wallace et al., 1995). Molecular dynamics trajectories were produced using CUDA designed code (*pmemd.cuda*) with computational facilities provided by the GPGPU Computing group at the Facultad de Matemática, Astronomía y Física (FAMAF), Universidad Nacional de Córdoba, Argentina.

3. Results and discussion

3.1. Method validation

The analytical method was fully validated according to the recommendations of the US Food and Drug Administration (FDA), the International Conference in Harmonization (ICH) and those of Shah et al. (2000). The following validation parameters were included: selectivity, linearity, limit of detection (LLOD), limit of quantification (LOQ), precision, accuracy, recovery and sample stability.

3.1.1. Selectivity

The selectivity of the method was evaluated by the analysis of both drug-free KRB and KRB samples containing low, medium and high concentrations (1.50×10^{-6}, 2.62×10^{-5} and 1.12×10^{-4} M, respectively) of 3TC, IS (AZT), 3TC-Etha and 3TC-Buta. In all cases, prior to the determination of selectivity, samples were subjected to the developed preparation procedure.

Based on the obtained results, this method proved to be selective, as no interferences were observed at the retention times of any of the analytes or of the extracted sample matrix.

3.1.2. Linearity and sensitivity (LOD, LLOQ)

The calibration curves for 3TC, 3TC-Etha and 3TC-Buta were constructed by fitting the analyte/IS area ratio vs. analyte/IS concentration ratio, using eight point calibrations in the range 1.50×10^{-6}–1.12×10^{-4} M. Acceptable criteria included correlation coefficients higher than 0.99. The slopes and intercepts were determined by the least-squares linear regression analysis method, which are shown in Table 1. To study the variability of the calibration parameters, calibration curves were obtained for 5 days over a 2 month period for a different set of standards.

The LOD and LLOQ were determined based on the standard deviation of the response and the calibration curve slopes. The LOD was defined as the lowest concentration of the analyte which originated a signal to noise ratio of 3, with the following calculated values being obtained: 4.37×10^{-7}, 8.34×10^{-7} and 1.00×10^{-7} M, for 3TC, 3TC-Etha and 3TC-Buta, respectively. The LLOQ was defined as the lowest concentration of the analyte in the sample that originated a signal to noise ratio of 10. The following limits were obtained: 6.58×10^{-7}, 1.08×10^{-6} and 5.80×10^{-7} M, for 3TC, 3TC-Etha and 3TC-Buta, respectively.

Table 1
Calibration parameters including the slope, intercept and regression coefficients (r^2) for 3TC, 3TC-Etha and 3TC-Buta.

Compound	Slope	Intercept	r^2
3TC	1.09 ± 0.02	0.02 ± 0.03	0.99
3TC-Etha	0.52 ± 0.02	0.01 ± 0.02	0.99
3TC-Buta	1.17 ± 0.03	0.02 ± 0.04	0.99

3.1.3. Precision and accuracy

Precision and accuracy were evaluated at three concentrations (low = 1.50×10^{-6}, medium = 2.62×10^{-5}, high = 1.12×10^{-4} M), and intra-day precision and accuracy were assessed by analyzing ten replicates at each concentration in the same run. To study the reproducibility of the method (inter-day repeatability), these three concentration levels were analyzed on 10 different days over a 2-month period involving different analysts.

Table 2 presents the results expressed as a percentage of the relative standard deviation (RSD, %) for the intra- and inter-day assays. The obtained results indicate that the method developed for quantitative analysis exhibited an adequate precision and accuracy.

3.1.4. Recovery

The recoveries of 3TC, 3TC-Etha and 3TC-Buta were determined by spiking KRB at the three concentration levels as described in Section 3.1.3. The resulting solutions were subjected to the reported sample preparation procedure and quantitative analysis, with the results expressed as the mean of ten replicate analyses (Table 3). It should be noted that recovery values higher that 100% are originated in the concentration and reconstitution step (200 μl) of the sample preparation procedure. These values are within the accepted validation criteria, and are corrected by the addition of the internal standard (AZT).

3.1.5. Sample stability

In order to study the stability of processed samples under storing conditions, solutions of 3TC-Etha and 3TC-Buta were prepared in KRB at the three concentration levels described in *3.1.3* and afterwards subjected to the sample preparation procedure. It is worth remarking that aqueous solubility values for 3TC, 3TC-Etha and 3TC-Buta (65.9, 8.56 and 1.13 mg/ml, respectively – data not yet published) were previously determined in our laboratory and granted that the assayed compounds did not precipitate in the mucosal solution. The concentrated samples were stored at 5 °C for 7 days, after which they were subjected to HPLC analyses. No statistical differences were found between stored samples and freshly prepared samples, revealing that no 3TC-Etha or 3TC-Buta degradation took place during sample storage.

3.2. 3TC-Etha and 3TC-Buta stability in KRB

The stability of 3TC-Etha and 3TC-Buta was determined in KRB under identical conditions as those used in the intestinal permeation assay (37 °C, carbogen gas, 60 min). After quantitation, no 3TC was detected in the assayed KRB solution, while the plots of the concentration of 3TC-Etha and 3TC-Buta (Fig. 2) showed that both compounds were stable under the assayed conditions.

Table 2
Intra- and inter-day precisions (RSD %) at the different sample concentrations obtained for 3TC, 3TC-Etha and 3TC-Buta.

Compound	Intra-day (RSD %)			Inter-day (RSD %)		
	1.50×10^{-6} M	2.62×10^{-5} M	1.12×10^{-4} M	1.50×10^{-6} M	2.62×10^{-5} M	1.12×10^{-4} M
3TC	0.82	0.38	0.15	3.74	4.51	3.28
3TC-Etha	2.30	0.54	0.80	1.31	1.86	1.80
3TC-Buta	1.32	0.34	0.22	3.34	1.85	0.12

Table 3
Recovery (%) obtained with the sample preparation technique for 3TC, 3TC-Etha and 3TC-Buta.

Compound	Recoveries (%)		
	1.50×10^{-6} M	2.62×10^{-5} M	1.12×10^{-4} M
3TC	85.4	112.5	103.6
3TC-Etha	95.9	95.7	106.2
3TC-Buta	109.1	104.8	95.7

3.3. Intestinal permeation of 3TC

The intestinal permeability of 3TC was studied at four mucosal drug concentrations (1.25, 1.64, 2.62 and 3.92 mM), which were selected considering the single human dose strength as indicated in a previous report (Mariappan and Singh, 2007) and aimed at obtaining mucosal 3TC concentrations in the range of a 0.48–1.5 dose strength. Fig. 3a shows the amount of 3TC that permeated through the jejunum in the A/B direction (everted mode) at the corresponding sampling intervals and at the four assayed concentrations.

As expected, the amount of drug permeated in all cases increased between 0 and 30 min (Fig. 3a), after which it remained constant throughout the experiment. This is in agreement with the diffusion equilibrium between drug concentration and the intestinal tissue needed to reach a steady state in the permeation process. Fig. 3b shows the amount of 3TC accumulated in the serosal solution as a result of permeation through the intestinal segments at the four assayed concentrations (1.25, 1.64, 2.62 and

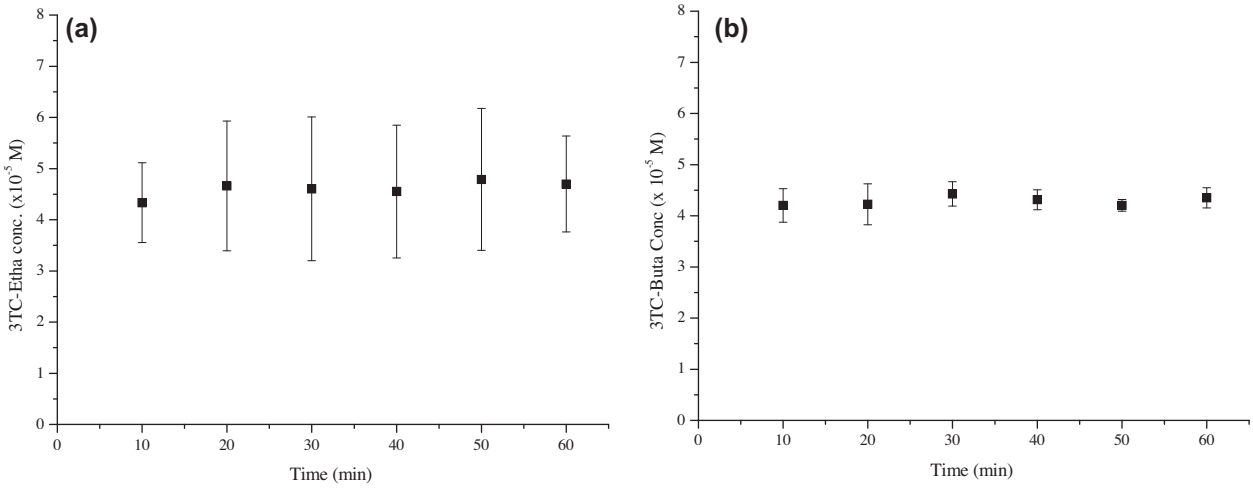

Fig. 2. Plots of the amounts of: (a) 3TC-Etha and (b) 3TC-Buta vs. time determined in the chemical stability (KRB) studies.

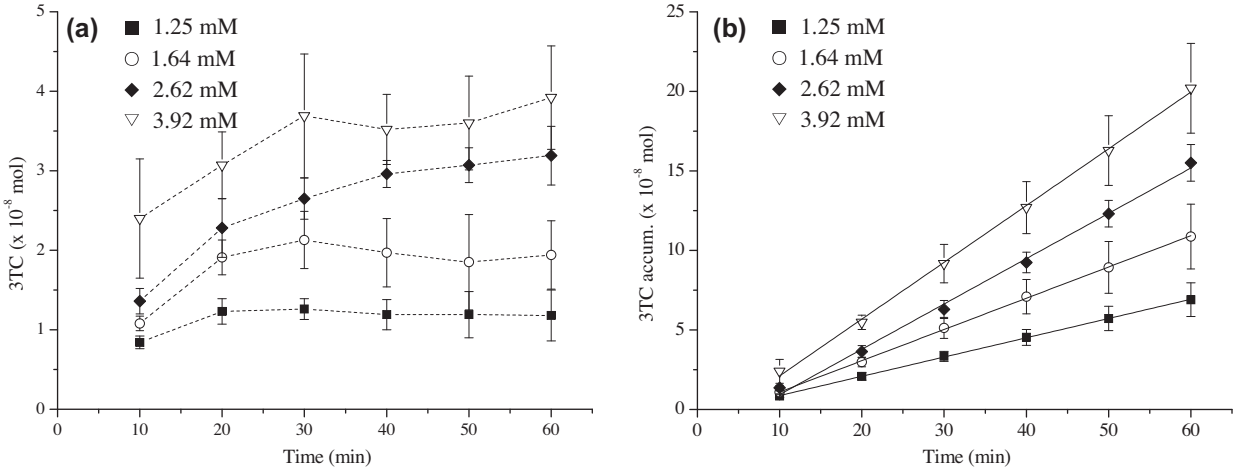

Fig. 3. (a) Amounts of 3TC that permeated through rat jejunum at each concentration and sampling time and (b) plots of the accumulated amounts of 3TC vs. time that permeated through rat jejunum.

Table 4
Permeability parameters calculated for the permeation of 3TC through rat jejunum in: (a) apical-to-basal direction, (b) apical-to-basal direction in the presence of VER and (c) basal-to-apical direction.

3TC Conc. (mM)	Lag time (min)	F ($\times 10^{-8}$ mol/min)	P_{app} ($\times 10^{-4}$ cm/min)
(a) 3TC – apical/basal			
1.25	2.69 (±1.46)	0.121 (±0.001)	0.388 (±0.064)
1.64	4.24 (±1.38)	0.196 (±0.002)	0.478 (±0.098)
2.62	6.73 (±0.74)	0.285 (±0.008)	0.406 (±0.032)
3.92	4.08 (±0.53)	0.357 (±0.006)	0.362 (±0.047)
(b) 3TC + verapamil (1×10^{-4} M) – apical/basal			
1.25	5.63 (±1.83)	0.052 (±0.001)	0.165 (±0.023)
(c) 3TC – basal/apical			
1.25	17.05 (±1.70)	0.109 (±0.016)	0.402 (±0.068)

3.92 mM, respectively). Linear regression analyses were performed (Eqs. (3)–(6)) with the corresponding lag times, F and P_{app} being calculated (Table 4a):

$$\begin{aligned}\text{3TC acc.}(\times 10^{-8}\ \text{mol}) &= 0.121\ (\pm 0.001)\ \text{Time (min)} \\ &\quad - 0.339\ (\pm 0.031) \\ n = 6;\ r^2 &= 0.999;\ \text{sd} = 0.033; F = 23259.9\end{aligned} \tag{3}$$

$$\begin{aligned}\text{3TC acc.}(\times 10^{-8}\ \text{mol}) &= 0.196\ (\pm 0.002)\ \text{Time (min)} \\ &\quad - 0.860\ (\pm 0.079) \\ n = 6;\ r^2 &= 0.999;\ \text{sd} = 0.085;\ F = 9425.9\end{aligned} \tag{4}$$

$$\begin{aligned}\text{3TC acc.}(\times 10^{-8}\ \text{mol}) &= 0.285(\pm 0.008)\ \text{Time (min)} \\ &\quad - 1.906\ (\pm 0.320) \\ = 6;\ r^2 &= 0.995;\ \text{sd} = 0.352; F = 1145.6\end{aligned} \tag{5}$$

$$\begin{aligned}\text{3TC acc.}(\times 10^{-8}\ \text{mol}) &= 0.357\ (\pm 0.006)\ \text{Time (min)} \\ &\quad - 1.455\ (\pm 0.217) \\ = 6;\ r^2 &= 0.999;\ \text{sd} = 0.233;\ F = 4107.95\end{aligned} \tag{6}$$

The permeability parameters for 3TC are shown in Table 4a, finding no statistical differences between the calculated P_{app} at the four assayed concentrations. This observation suggests the involvement of a passive diffusion mechanism in 3TC permeation through the intestinal tissue as measured applying this permeability model. However, in order to definitively asses the absorptive mechanism involved for 3TC, additional data from complementary permeability techniques (such as PAMPA assays) are required.

The mean P_{app} determined for 3TC at the assayed concentrations was 0.408 (±0.049) $\times 10^{-4}$ cm/min, which if compared to the recently reported value for another NRTI, AZT ($2.38 \pm 0.12 \times 10^{-4}$ cm/min) (Quevedo et al., 2011), an almost 6 times less permeability was found for the former molecule. The lower intestinal permeability of 3TC compared to that of AZT may have originated due to the fact that 3TC is a more hydrophilic molecule than AZT ($\text{Log}P_{o/w} = -0.91$ and 0.02, respectively) (Moroni et al., 2002; Ravetti et al., 2008). After calculating the corresponding lag times, no statistical differences were found for any of the four assayed concentrations, suggesting that the equilibration of 3TC concentration across the intestinal segment was mainly determined by the mucosal surface absorption area.

To assess whether 3TC permeability may also be impaired by efflux mechanisms mediated by the ATP-binding cassette (ABC) family of proteins (Szakacs et al., 2008), permeation assays were performed in the presence of VER (1×10^{-4} M), a well known P-gp and MRP-1 inhibitor (Breedveld et al., 2006; Dahan and Amidon, 2009). It has been previously reported that P-gp is selectively expressed on the apical side of the enterocyte, while MRP-1 is expressed on the basal side (Zhou, 2008). Consequently, VER was only added to the mucosal solution (apical side) to be able to selectively study the inhibition of P-gp. After the corresponding linear regression analysis was performed (Eq. (7)), the lag time, F and P_{app} were calculated (Table 4b):

$$\begin{aligned}\text{3TC acc.}(\times 10^{-8}\ \text{mol}) &= 0.052\ (\pm 0.001)\ \text{Time (min)} \\ &\quad - 0.296\ (\pm 0.032) \\ n = 6;\ r^2 &= 0.999;\ \text{sd} = 0.035;\ F = 3837.7\end{aligned} \tag{7}$$

A lower permeability was found for 3TC in the presence of VER ($p > 0.05$), demonstrating that 3TC was not a substrate of the P-gp located in the apical side of the enterocyte. This finding is in agreement with the current knowledge regarding the physicochemical properties of P-gp substrates, since, as previously pointed out, 3TC is a hydrophilic molecule and the partitioning into the lipid membrane is the rate limiting step of the efflux process (Szakacs et al., 2008; Zhou, 2008). In addition, no statistical differences between the calculated lag times were found in the presence or absence of the inhibitor.

Permeability of 3TC was also evaluated in the B/A (non-everted) direction at a 1.25 mM mucosal drug concentration. After performing quantitative analyses, Eq. (8) was obtained and the corresponding permeability parameters were calculated (Table 4c):

$$\begin{aligned}\text{3TC acc.}(\times 10^{-8}\ \text{mol}) &= 0.110\ (\pm 0.016)\ \text{Time (min)} \\ &\quad - 1.802\ (\pm 0.630) \\ n = 6;\ r^2 &= 0.991;\ \text{sd} = 0.675;\ F = 46.42\end{aligned} \tag{8}$$

No statistical differences ($p > 0.05$) were found between F and P_{app} in the A/B or B/A directions, indicating that 3TC was not a substrate of the ABC transporters located on the basal side of the enterocyte. It is noteworthy that in the B/A direction the lag time was sixfold higher than that calculated for the A/B permeation (17.05 ± 1.70 and 2.69 ± 1.46, respectively), which may have been a consequence of the lower absorptive surface area of the basal membrane compared to that of the mucosal brush border in the enterocyte. In this way, although the overall permeability was equivalent in both directions, it took a longer time for 3TC to equilibrate drug concentrations through the intestinal tissue from the basal to the apical compartment. When considering the sink conditions that are present *in vivo* due to intestinal blood flow, it can be assumed that the observed differences in permeation lag times may enhance 3TC absorption. This hypothesis is in line with the relatively high bioavailability reported for 3TC (Strauch et al., 2011).

3.4. Intestinal permeation of 3TC-Etha

The permeability of 3TC-Etha was only studied at mucosal drug concentrations of 1.25 and 1.64 mM, since at higher drug levels the complete dissolution of the compound in the KRB media was not achieved. When the intestinal permeability was studied in the A/B direction, it was found that only a small fraction of 3TC-Etha was able to permeate through the intestinal tissue, although significant amounts of 3TC were quantified in the serosal solution. Consequently, the corresponding F and P_{app} for the intact compound and the regenerated 3TC were calculated at 1.25 mM (Eqs. (9) and (10), respectively) and 1.64 mM (Eqs. (11) and (12), respectively) and are summarized in Table 5a:

Table 5
Permeability parameters calculated for the permeation of 3TC-Etha and regenerated 3TC through rat jejunum in: (a) apical-to-basal direction, (b) apical-to-basal direction in the presence of verapamil and (c) basal-to-apical direction.

3TC-Etha Conc. (mM)		Lag time (min)	F ($\times 10^{-8}$ mol/min)	P_{app} ($\times 10^{-4}$ cm/min)
(a) 3TC-Etha – apical/basal				
1.25	3TC-Etha	7.15 (±2.23)	0.031 (±0.002)	0.093 (±0.010)
	3TC-Etha → 3TC	5.62 (±0.27)	0.301 (±0.008)	0.733 (±0.131)
1.64	3TC-Etha	6.32 (±1.09)	0.065 (±0.013)	0.159 (±0.081)
	3TC-Etha → 3TC	5.92 (±0.63)	0.392 (±0.010)	0.725 (±0.078)
(b) 3TC-Etha + verapamil (1×10^{-4} M) – apical/basal				
1.25	3TC-Etha	4.65 (±0.58)	2.170 (±0.122)	6.933 (±0.586)
	3TC-Etha → 3TC	5.84 (±1.45)	0.331 (±0.012)	1.057 (±0.123)
(c) 3TC-Etha – basal/apical				
1.25	3TC-Etha	12.87 (±2.11)	0.892 (±0.060)	2.851 (±0.723)
	3TC-Etha → 3TC	20.17 (±1.30)	0.048 (±0.006)	0.153 (±0.012)

$$\text{3TC-Etha acc.}(\times 10^{-8}\,\text{mol}) = 0.031\ (\pm 0.001)\,\text{Time (min)} - 0.213\ (\pm 0.060)$$
$$n = 6;\ r^2 = 0.988;\ \text{sd} = 0.062;\ F = 431.47 \quad (9)$$

$$\text{3TC acc.}(\times 10^{-8}\,\text{mol}) = 0.301\ (\pm 0.008)\ \text{Time (min)} - 1.700\ (\pm 0.295)$$
$$n = 6;\ r^2 = 0.997;\ \text{sd} = 0.317;\ F = 1582.72 \quad (10)$$

$$\text{3TC-Etha acc.}(\times 10^{-8}\,\text{mol}) = 0.065\ (\pm 0.002)\,\text{Time (min)} - 0.462\ (\pm 0.098)$$
$$n = 6;\ r^2 = 0.993;\ \text{sd} = 0.105;\ F = 679.06 \quad (11)$$

$$\text{3TC acc.}(\times 10^{-8}\,\text{mol}) = 0.392\ (\pm 0.010)\ \text{Time (min)} - 2.320\ (\pm 0.389)$$
$$n = 6;\ r^2 = 0.998;\ \text{sd} = 0.418;\ F = 1541.47 \quad (12)$$

At a 1.25 mM drug concentration low values of F and P_{app} were found for 3TC-Etha (0.031 ± 0.002 and 0.093 ± 0.010, respectively). The same behavior was observed at a mucosal drug concentration of 1.64 mM, with F and P_{app} values of 0.037 (±0.003) and 0.159 (±0.081), respectively, and no statistical differences were found between the calculated parameters at both concentrations. The low permeability of this compound may have originated from a high rate of enzymatic hydrolysis during its permeation through the intestinal tissue, from the presence of an efflux mechanism taking place on the apical side of the enterocyte, or through a combination of both these phenomena. After calculating the permeability of 3TC regenerated from 3TC-Etha at 1.25 mM mucosal drug concentration, a twofold increase ($p < 0.05$) was found in the corresponding P_{app} when compared to the value determined for 3TC at the same drug concentration (0.733 ± 0.010 and 0.388 ± 0.064, respectively). This suggests that 3TC-Etha was able to permeate more rapidly than 3TC through the apical membrane of the enterocyte, before being hydrolyzed in the cellular lumen and regenerating the 3TC that afterwards permeated through the basal membrane into the serosal solution (Fig. 4). The same behavior was observed at the higher 3TC-Etha concentration (1.64 mM), with no statistical differences between the P_{app} calculated for the 3TC regenerated from 3TC-Etha being observed. With respect to the calculated lag times, no differences were found among 3TC-Etha, regenerated 3TC and 3TC alone.

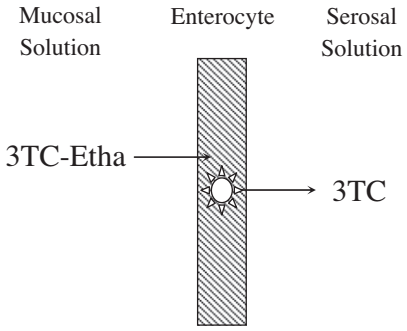

Fig. 4. Graphical representation of the processes involved in 3TC-Etha intestinal permeation.

To investigate further the involvement of ABC transporters in 3TC-Etha permeability, VER (1×10^{-4} M) was added to the mucosal solution (1.25 mM) in the A/B permeation model. After performing quantitative analyses (Eqs. (13) and (14)), the corresponding permeability parameters for 3TC-Etha and the regenerated 3TC were calculated (Table 5b):

$$\text{3TC-Etha acc.}(\times 10^{-8}\,\text{mol}) = 2.170\ (\pm 0.122)\,\text{Time (min)} - 10.148\ (\pm 4.470)$$
$$n = 6;\ r^2 = 0.984;\ \text{sd} = 0.591;\ F = 317.67 \quad (13)$$

$$\text{3TC acc.}(\times 10^{-8}\,\text{mol}) = 0.330\ (\pm 0.012)\ \text{Time (min)} - 1.913\ (\pm 0.478)$$
$$n = 6;\ r^2 = 0.993;\ \text{sd} = 0.513;\ F = 726.19 \quad (14)$$

In this case considerable amounts of 3TC-Etha were found in the serosal solution, with the calculated values of F and P_{app} being 2.170 (±0.122) and 6.933 (±0.586), respectively (Table 5b). This represents a 74-fold increase in 3TC-Etha permeability compared to that in the absence of the P-gp inhibitor, which demonstrates that this compound is a substrate of P-gp and that this ABC protein was responsible for the low permeability of this compound. The fact that 3TC-Etha was subjected to a P-gp mediated active efflux is consistent the enhanced lipophilicity of this drug with respect to 3TC (−0.31 and −0.91, respectively) (Ravetti et al., 2008). After calculating the permeability parameters for 3TC regenerated from 3TC-Etha (Table 5b), a slightly higher permeability was observed in

the presence of the inhibitor. In addition, no significant differences between the lag times for the prodrug and 3TC were found, indicating that the time needed to equilibrate the drug concentration through the enterocyte membrane was not dependent on the drug lipophilicity or the concentration.

With the aim of evaluating wether 3TC-Etha may also have been subjected to active efflux on the basal side of the enterocyte, permeation experiments were conducted in the non-everted mode. From the regression analysis (Eqs. (15) and (16)) and the calculated permeability coefficients (Table 5c), an A/B vs. B/A permeability ratio of 0.034 was calculated, which demonstrates that 3TC-Etha was effectively subjected to efflux transport on the basal side of the enterocyte. It is important to note that low amounts of 3TC reached the mucosal solution, demonstrating that no significant hydrolysis of 3TC-Etha took place when this derivative permeated in the B/A direction:

$$\begin{aligned}\text{3TC-Etha acc.}(\times 10^{-8}\,\text{mol}) &= 0.892\ (\pm 0.060)\ \text{Time (min)} \\ &\quad - 11.239\ (\pm 2.335) \\ n = 6;\ r^2 &= 0.979;\ \text{sd} = 0.250;\ F = 221.41\end{aligned} \tag{15}$$

$$\begin{aligned}\text{3TC acc.}(\times 10^{-8}\,\text{mol}) &= 0.047\ (\pm 0.006)\ \text{Time (min)} \\ &\quad - 0.704\ (\pm 0.250) \\ n = 6;\ r^2 &= 0.975;\ \text{sd} = 0.269;\ F = 54.76\end{aligned} \tag{16}$$

3.5. Intestinal permeation of 3TC-Buta

As previously described for 3TC-Etha, when the permeation of 3TC-Buta was evaluated at mucosal drug concentrations of 1.25 and 1.64 mM, only a small amount of the intact compound was able to permeate through the intestinal tissue. Again, the corresponding amounts of accumulated drug vs. time and permeation constants were calculated for both 3TC-Buta and regenerated 3TC (Eqs. (17)–(20), Table 6):

$$\begin{aligned}\text{3TC-Buta acc.}(\times 10^{-8}\,\text{mol}) &= 0.026\ (\pm 0.001)\ \text{Time (min)} \\ &\quad - 0.276\ (\pm 0.019) \\ n = 6;\ r^2 &= 0.998;\ \text{sd} = 0.020;\ F = 2891.18\end{aligned} \tag{17}$$

$$\begin{aligned}\text{3TC acc.}(\times 10^{-8}\,\text{mol}) &= 1.110\ (\pm 0.071)\ \text{Time (min)} \\ &\quad - 2.885\ (\pm 1.773) \\ n = 6;\ r^2 &= 0.979;\ \text{sd} = 0.298;\ F = 242.33\end{aligned} \tag{18}$$

$$\begin{aligned}\text{3TC-Buta acc.}(\times 10^{-8}\,\text{mol}) &= 0.035\ (\pm 0.001)\ \text{Time (min)} \\ &\quad - 0.257\ (\pm 0.021) \\ n = 6;\ r^2 &= 0.999;\ \text{sd} = 0.023;\ F = 4277.37\end{aligned} \tag{19}$$

$$\begin{aligned}\text{3TC acc.}(\times 10^{-8}\,\text{mol}) &= 2.600\ (\pm 0.110)\ \text{Time (min)} \\ &\quad - 13.395\ (\pm 4.273) \\ n = 6;\ r^2 &= 0.991;\ \text{sd} = 0.458;\ F = 561.29\end{aligned} \tag{20}$$

As shown in Table 6a, 3TC-Buta exhibited a low permeability in the A/B direction, with a calculated F of 0.026 ± 0.001 and 0.035 ± 0.001 at 1.25 and 1.64 mM, respectively. Correspondingly, low P_{app} values were also found, with results of 0.090 ± 0.030 and 0.123 ± 0.043 at drug levels of 1.25 and 1.64 mM, respectively. As was the case for 3TC-Etha, the low permeability of this prodrug may have been originated from its susceptibility to enzymatic hydrolysis within the intestinal tissue, from the involvement of efflux mechanisms, or through a combination of both these phenomena. In addition, high amounts of 3TC were quantified in the serosal solution as a consequence of 3TC-Buta hydrolysis, with F and P_{app} at a 1.25 mM mucosal drug concentration having values of 1.110 ± 0.071 and 2.054 ± 0.481, respectively, while those calculated at a 1.64 mM mucosal drug concentration were 2.600 ± 0.110 and 4.807 ± 0.901, respectively. Based on these observations, we conclude that this prodrug was able to considerably increase 3TC intestinal permeability compared to 3TC alone, with a 5-fold increase found in the P_{app} ($p < 0.05$) at 1.25 mM and a 10-fold increase ($p < 0.05$) observed at 1.65 mM. Moreover, the enhancement in 3TC permeability was higher than that observed for 3TC-Etha, a fact that was consistent with the enhanced lipophilicity of 3TC-Buta with respect to 3TC and 3TC-Etha ($\text{Log}P_{o/w}$ 0.86, −0.31 and −0.91, respectively) (Ravetti et al., 2008). Statistical analyses also demonstrated a concentration dependent permeability of the 3TC regenerated from 3TC-Buta, but this phenomenon was not further investigated in the present study.

To assess if the low permeability found for 3TC-Buta responded to the presence of efflux mechanisms, permeation assays were per-

Table 6
Permeability parameters calculated for the permeation of 3TC-Butha and regenerated 3TC through rat jejunum in: (a) apical-to-basal direction, (b) apical-to-basal direction in the presence of verapamil and (c) basal-to-apical direction.

3TC-Buta Conc. (mM)		Lag time (min)	F ($\times 10^{-8}$ mol/min)	P_{app} ($\times 10^{-4}$ cm/min)
(a) 3TC-Buta – apical/basal				
1.25	3TC-Buta	13.37 (±2.79)	0.026 (±0.001)	0.090 (±0.030)
	3TC-Buta → 3TC	1.31 (±0.29)	1.110 (±0.071)	2.054 (±0.481)
1.64	3TC-Buta	6.86 (±2.13)	0.035 (±0.001)	0.123 (±0.043)
	3TC-Buta → 3TC	5.00 (±0.69)	2.600 (±0.110)	4.807 (±0.901)
b) 3TC-Buta + verapamil (1×10^{-4} M) – apical/basal				
1.25	3TC-Buta	9.13 (±1.80)	0.029 (±0.003)	0.106 (±0.020)
	3TC-Buta → 3TC	2.48 (±0.30)	1.386 (±0.160)	2.562 (±0.202)
(c) 3TC-Buta + quercetin (1×10^{-4} M) – apical/basal				
1.25	3TC-Buta	15.30 (±0.50)	0.014 (±0.001)	0.048 (±0.022)
	3TC-Buta → 3TC	7.44 (±2.46)	1.446 (±0.034)	4.881 (±0.921)
(d) 3TC-Buta – basal/apical				
1.25	3TC-Buta	12.61 (±2.25)	0.157 (±0.009)	0.558 (±0.088)
	3TC-Buta → 3TC	15.32 (±1.12)	0.093 (±0.014)	0.227 (±0.059)

formed in the presence of VER, and the corresponding F and P_{app} values for the prodrug and the 3TC regenerated were calculated (Eqs. (21) and (22), Table 6b):

$$\text{3TC-Buta acc.}(\times 10^{-8}\, mol) = 0.029\,(\pm 0.001)\,\text{Time (min)} - 0.303\,(\pm 0.021)$$
$$n = 6;\ r^2 = 0.998;\ \text{sd} = 0.022;\ F = 2950.71 \quad (21)$$

$$\text{3TC acc.}(\times 10^{-8}\ \text{mol}) = 1.386\ (\pm 0.160)\ \text{Time (min)} - 5.178\ (\pm 2.358)$$
$$n = 6;\ r^2 = 0.990;\ \text{sd} = 0.253;\ F = 524.31 \quad (22)$$

In contrast to what was observed for 3TC-Etha, no significant increase in 3TC-Buta permeability was found in the presence of VER, with no statistical differences ($p > 0.05$) observed between the F and P_{app} values of the intact prodrug or regenerated 3TC compared to those calculated in absence of the inhibitor. This finding indicates that, in contrast to what was found for 3TC-Etha, 3TC-Buta was not a substrate of P-gp on the basal side of the enterocyte. To assess if the breast cancer resistance protein (BCRP) efflux transporter may have been involved (Szakacs et al., 2008), the permeation study was also performed in the presence of QUE (1×10^{-4} M), a well know inhibitor of this protein (Robey et al., 2009). The corresponding permeability coefficients were calculated and are shown in Table 6c. As in the case of the previous experimental design, 3TC-Buta was still not able to permeate through the intestinal tissue, leading to the conclusion that BCRP was not involved in the 3TC-Buta efflux. Based on these findings it can be concluded that the high levels of regenerated 3TC quantified in the serosal solutions were due to a high susceptibility of 3TC-Buta to enzymatic hydrolysis in the lumen of the enterocyte.

When the permeation of 3TC-Buta was assayed in the B/A direction, an increased permeability was found for the intact compound (Eqs. (23) and (24)), with F and P_{app} values of 0.157 ± 0.009 and 0.558 ± 0.088, respectively. However, since the amount of 3TC regenerated during the permeation process was significantly lower, it is suggested that 3TC-Buta may have been hydrolyzed principally by the esterases located at the mucosal brush border. The B/A permeability behavior of 3TC-Buta was homologous to that observed for 3TC-Etha, suggesting that both of these prodrugs were subjected to some extent to efflux at the basal side of the enterocyte, although additional studies are still needed to identify these transporters.

$$\text{3TC acc.}(\times 10^{-8}\ \text{mol}) = 0.093\ (\pm 0.014)\ \text{Time (min)} - 1.520\ (\pm 0.532)$$
$$n = 6;\ r^2 = 0.951;\ \text{sd} = 0.571;\ F = 143.61 \quad (23)$$

$$\text{3TC-Buta acc.}(\times 10^{-8}\,\text{mol}) = 0.157\,(\pm 0.010)\,\text{Time (min)} - 1.979\,(\pm 0.353)$$
$$n = 6;\ r^2 = 0.983;\ \text{sd} = 0.380;\ F = 299.19 \quad (24)$$

From the results presented above, it can be concluded that both 3TC-Etha and 3TC-Buta were able to enhance 3TC intestinal permeability, which is a relevant feature in their potential as 3TC prodrugs. However none of these compounds were able to permeate through the intestinal segment in their intact form, thus implying a limitation for the systemic biodistribution of these prodrugs if administered orally. As was previously described, 3TC-Etha was able to resist intestinal metabolism but unfortunately was subjected to P-gp mediated efflux. On the other hand, 3TC-Buta was not subjected to efflux mechanisms on the apical side of the enterocyte, but it was efficiently hydrolyzed in the intestinal brush border. In the light of these results, it is of particular interest to elucidate further details concerning the molecular basis which conferred such different behaviors of the two assayed prodrugs towards P-gp efflux. Clearly, a desired property would be to combine 3TC-Etha stability with the 3TC-Buta's ability to bypass the mucosal efflux transporters. Therefore, molecular modeling techniques were now applied to study the intermolecular recognition

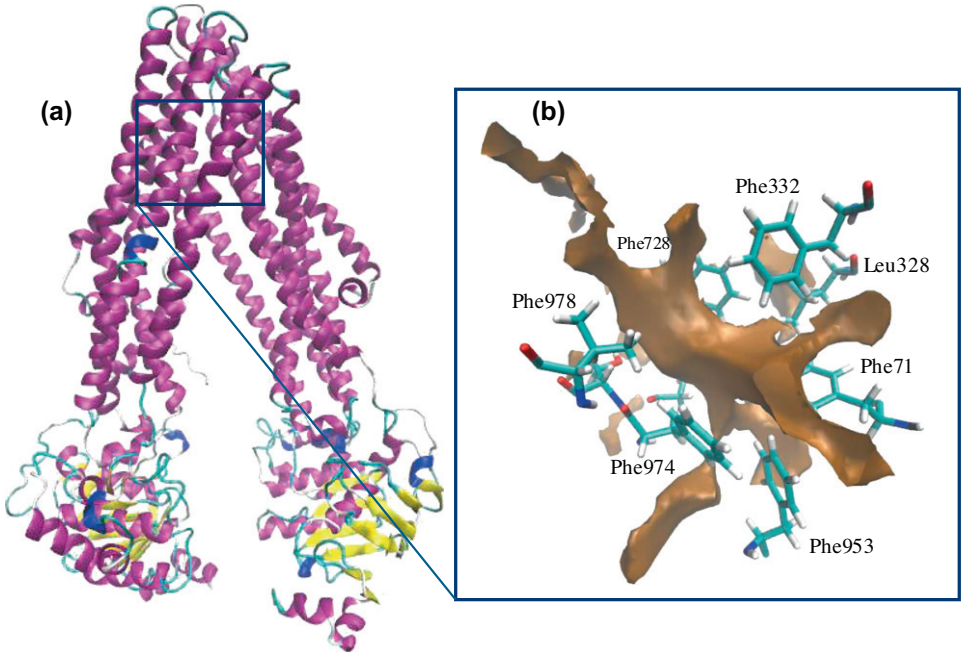

Fig. 5. (a) Location and (b) topological description of the verapamil binding site in P-gp. The main hydrophobic cavity inside the substrate binding site is depicted as a brown solid surface. (For interpretation of the references to color in this figure legend, the reader is referred to the web version of this article.)

between P-gp and a series of P-gp substrates belonging to the family of the NRTIs, which was afterwards compared to that of 3TC, 3TC-Etha and 3TC-Buta.

3.6. Binding to P-glycoprotein

3.6.1. Molecular docking studies

The drug binding site in P-gp was studied considering the *apo* protein crystal structure reported by Aller et al. (2009), with molecular docking procedures being performed on the reported VER binding site. From the binding site topological analyses (Fig. 5), it can be seen that the binding site is mainly formed by a large hydrophobic pocket, lined by residues Phe71, Leu328, Phe332, Phe728, Phe953, Phe974 and Phe978. To investigate the binding mode of the studied P-gp substrates, the binding poses of rhodamine 123, zidovudine and abacavir in the VER binding site of P-gp were studied, and afterwards compared to the binding modes of 3TC, 3TC-Etha and 3TC-Buta.

Regarding the binding mode of rhodamine 123 (Fig. 6a), it can be observed that this compound was able to position the hydrophobic region of the molecule within the main hydrophobic cavity inside the binding pocket. Consequently, it was possible to establish Van der Waals interactions with residues Phe71, Phe332, Phe728, Phe974, Val978 and Ala981 (Fig. 6b), suggesting that this binding mode may be a requirement for P-gp substrates.

AZT has also been recognized as a P-gp substrate (Quevedo et al., 2011), which is consistent with its predicted binding mode, where the hydrophobic pyrimidine ring is inserted into the main hydrophobic cavity (Fig. 7a), thereby establishing Van der Waals contacts with Phe71, Phe332, Phe724, Ser725, Phe728, Phe974, Ser975 and Val978 (Fig. 7b).

Abacavir is another NRTI that has been reported to be a substrate of P-gp (Shaik et al., 2007), with this feature being consistent with the binding mode obtained by molecular modeling methods (Fig. 8a), in which almost the whole molecule fits into the hydrophobic binding cavity of the binding site and is able to establish most of the previously reported Van der Waals contacts (Fig. 8b).

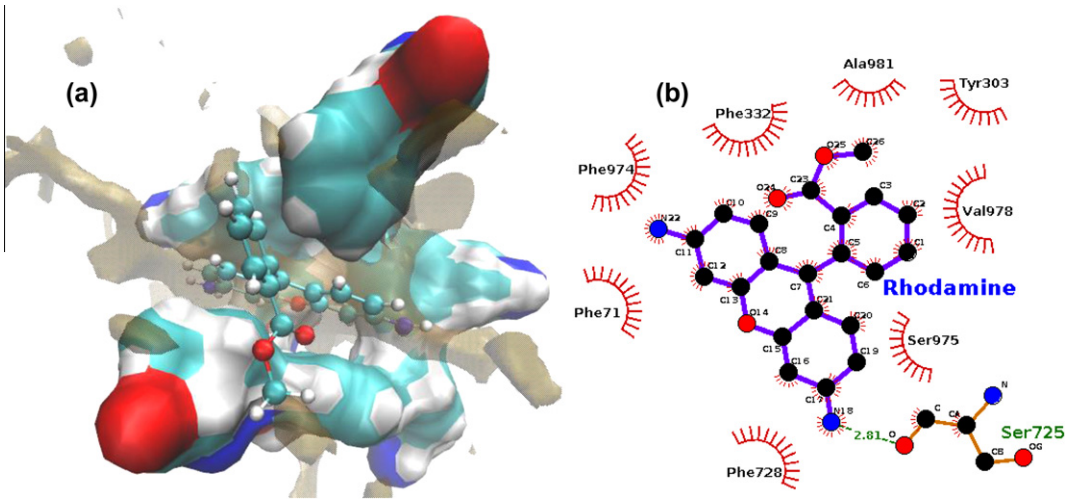

Fig. 6. (a) Binding mode of rhodamine 123 in the hydrophobic cavity of the P-gp binding site. (b) Main intermolecular interactions between rhodamine 123 and the residues lining the P-gp binding site cavity.

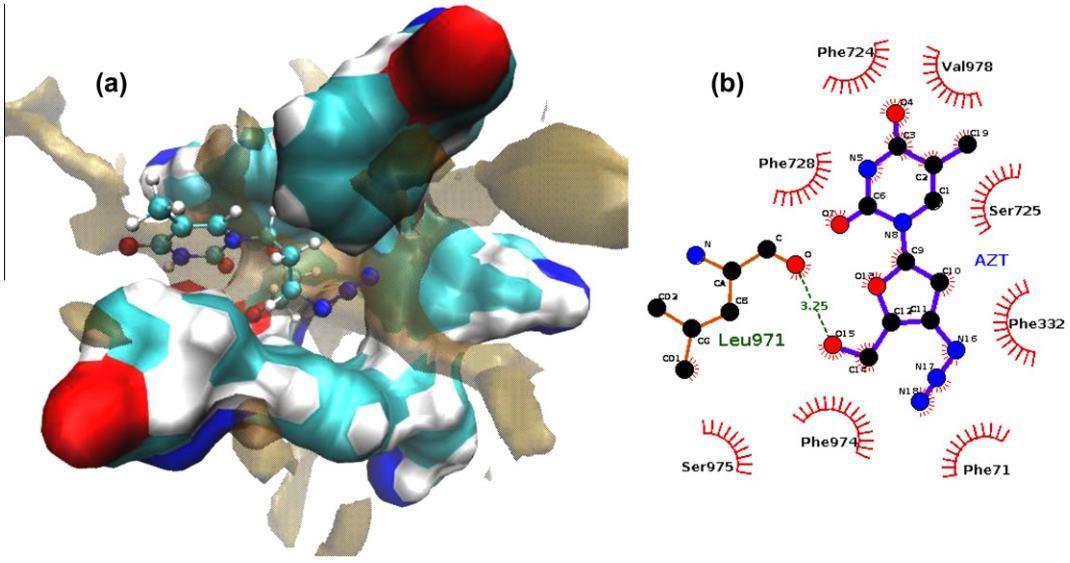

Fig. 7. (a) Binding mode of AZT in the hydrophobic cavity of the P-gp binding site. (b) Main intermolecular interactions between AZT and the residues lining the P-gp binding site cavity.

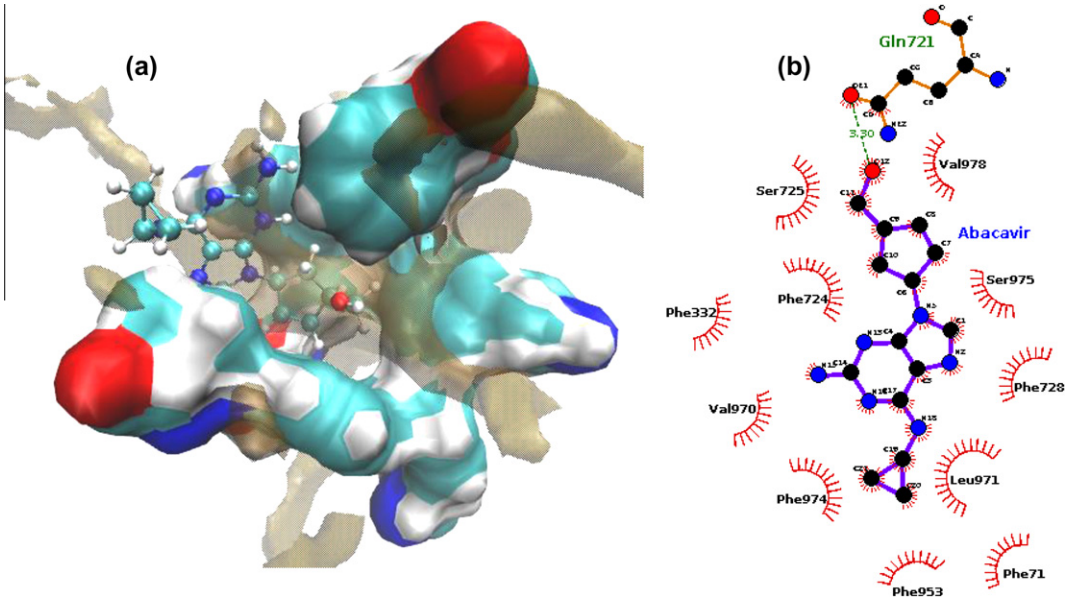

Fig. 8. (a) Binding mode of the NRTI abacavir in the hydrophobic cavity of the P-gp binding site. (b) Main intermolecular interactions between abacavir and the residues lining the P-gp binding site cavity.

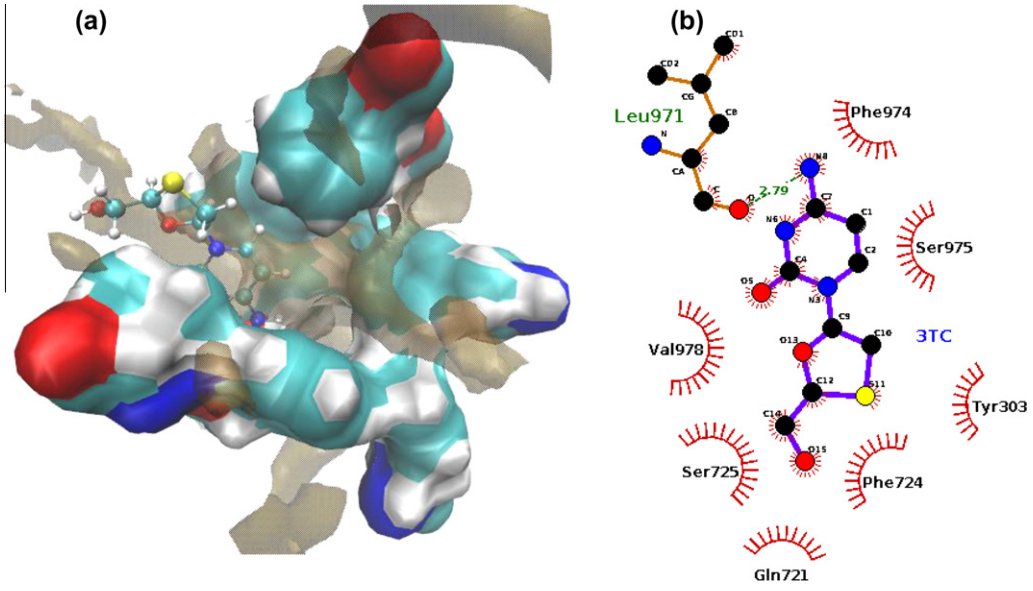

Fig. 9. (a) Binding mode of 3TC in the hydrophobic cavity of the P-gp binding site. (b) Main intermolecular interactions between 3TC and the residues lining the P-gp binding site cavity.

When the binding of 3TC was studied (Figs. 9a and b), we concluded that this molecule was able to bind into the substrate cavity in a similar way to that of the two previously studied NNRTI, and thus may be considered as a P-gp substrate. However, our experimental studies demonstrated that this compound was not a P-gp substrate, which suggests that although the molecule may be able to fit into the substrate binding site, it might not have possessed enough lipophilicity to reach this transmembrane region.

Regarding the binding mode of 3TC-Etha (Fig. 10a), the moiety corresponding to 3TC was deeply buried into the hydrophobic cavity of the binding site (Fig. 10b) and established Van der Waals interactions with most of the previously described aromatic residues, while the alcohol moiety was oriented toward a less hydrophobic cavity in the proximities of Met68 and Ile336. As part of our experimental studies it was confirmed that 3TC-Etha was a P-gp substrate (Table 5b), which is in agreement with it having a similar binding mode to that of rhodamine 123, AZT and abacavir. Also the increased lipophilicity of 3TC-Etha with respect to 3TC seemed to be sufficient for the molecule to reach the transmembrane binding site.

When the binding of 3TC-Buta was determined (Fig. 11a), a completely different binding mode to those obtained for typical P-gp substrates was found. In this case, the buthanol moiety was deeply inserted into the hydrophobic cavity and established Van der Waals contacts with the main aromatic residues, while the 3TC moiety was oriented facing outwards from the cavity (Fig. 10b). This binding mode has not been previously observed for the P-gp substrates previously described, and consequently, it was not possible to define whether a substrate may have bound in this orientation or if this was not energetically possible. Further

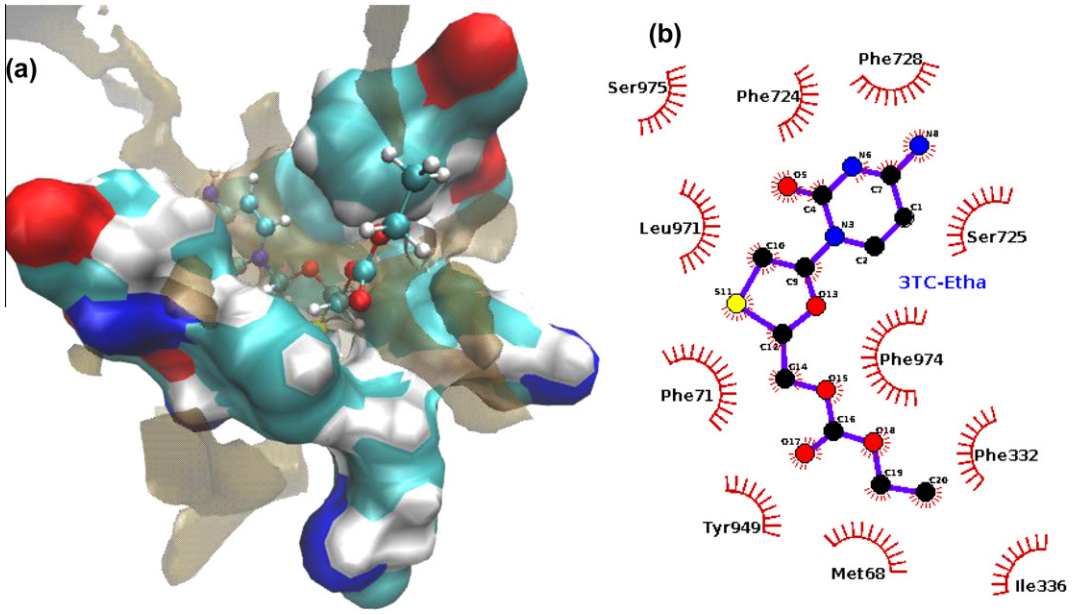

Fig. 10. (a) Binding mode of 3TC-Etha in the hydrophobic cavity of the P-gp binding site. (b) Main intermolecular interactions between 3TC-Etha and the residues lining the P-gp binding site cavity.

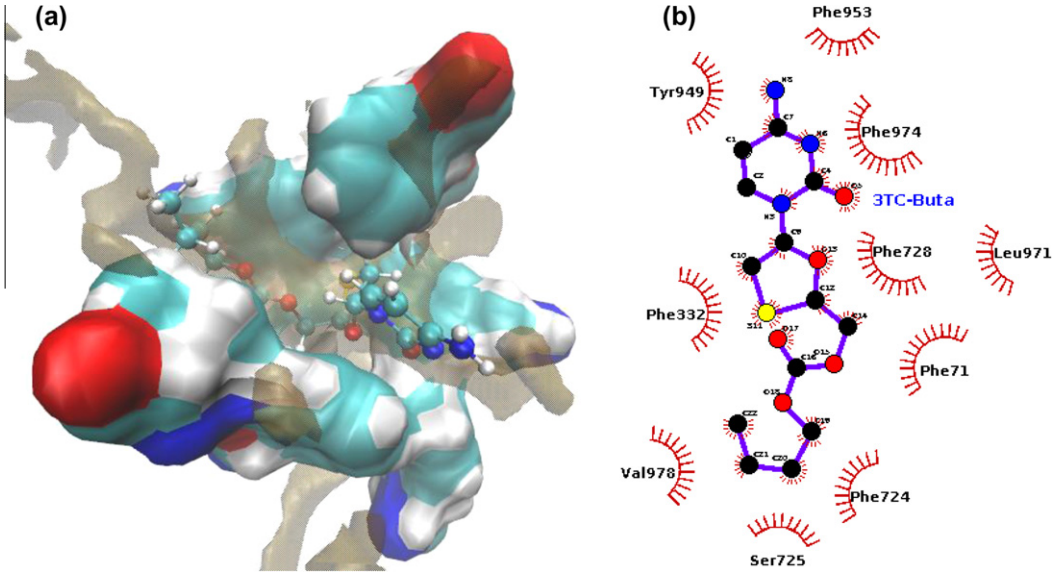

Fig. 11. (a) Binding mode of 3TC-Buta in the hydrophobic cavity of the P-gp binding site. (b) Main intermolecular interactions between 3TC-Buta and the residues lining the P-gp binding site cavity.

comparisons between the binding poses obtained for 3TC-Etha and 3TC-Buta were now carried out by molecular dynamics methods.

3.6.2. Molecular dynamics analyses

The quality of the molecular dynamics trajectories obtained was checked by evaluation of the corresponding temperatures, and the potential, kinetic and total energy values over the 250–425 ps simulation interval (as an example, Figs. 12 and 13 show the plots obtained for 3TC-Etha).

No abnormal values were found, indicating that the trajectories were adequately obtained and equilibrated, thus further structural and energetic analyses were performed. After heating, the equilibration and production phases were completed, energetic component analyses were performed on the trajectory corresponding to the 250–425 ps time interval, with the corresponding results presented in Table 7.

As shown in Table 7, the binding of both compounds to P-gp was mainly stabilized by hydrophobic forces (with values of −40.32 and −38,97 kcal/mol for 3TC-Etha and 3TC-Buta, respectively), while in the case of 3TC-Etha a significant additional stabilization was gained through the electrostatic component (−14.67 kcal/mol). However, for 3TC-Buta, no stabilization through this last component was found (−0.74 ± 2.85), which suggests that some kind of electrostatic repulsion was present. From the energetic residue decomposition analyses (data not shown), it was found that the electrostatic stabilization of 3TC-Etha was conferred mainly by a hydrogen bond between the carbonyl oxygen if the pyrimidine ring and the hydroxyl sidechain of Ser725 (Fig. 14a),

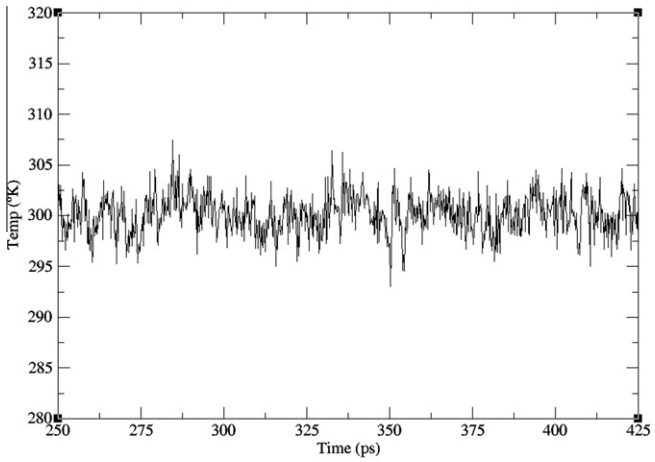

Fig. 12. Plot of the temperature vs. time (250–425 ps) obtained for the molecular dynamics trajectories of the complex between P-gp and 3TC-Etha.

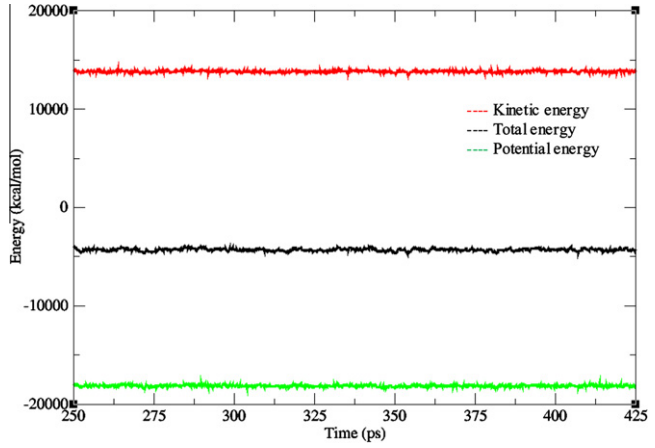

Fig. 13. Plots of the kinetic (red), potential (green) and total (black) energies obtained for the molecular dynamics trajectories of the complex between P-gp and 3TC-Etha (250–425 ps). (For interpretation of the references to color in this figure legend, the reader is referred to the web version of this article.)

Table 7
Energetic components for the binding of 3TC-Etha and 3TC-Buta to P-gp obtained by applying the Poisson–Boltzmann surface area (MM-PBSA) method.

Energetic component	3TC-Etha:P-gp	3TC-Buta:P-gp
ELE[a]	−14.67 (±4.52)	−0.74 (±2.85)
VDW[b]	−40.32 (±2.13)	−38.97 (±1.93)
GAS[c]	−54.98 (±4.53)	−39.71 (±3.78)
GBSUR[d]	−5.31 (±0.14)	−5.10 (±0.21)
GB[e]	30.46 (±2.92)	19.40 (±2.54)
GBSOL[f]	25.15 (±2.94)	14.31 (±2.7)
GBTOT[g]	−29.83 (±3.00)	−25.40 (±2.92)

[a] Electrostatic energy.
[b] van der Waals energy.
[c] Gas phase energy contribution (ELE + VDW).
[d] Non-polar contribution to the solvation free energy.
[e] Electrostatic contribution to the solvation free energy.
[f] sum of polar and non-polar contributions.
[g] final estimated binding free energy.

which maintained an interatomic distance below 3 Å approximately throughout the simulation (Fig. 14b). When the energetic decomposition analysis was performed for 3TC-Buta (data not shown), not only were no hydrogen bonds encountered when the

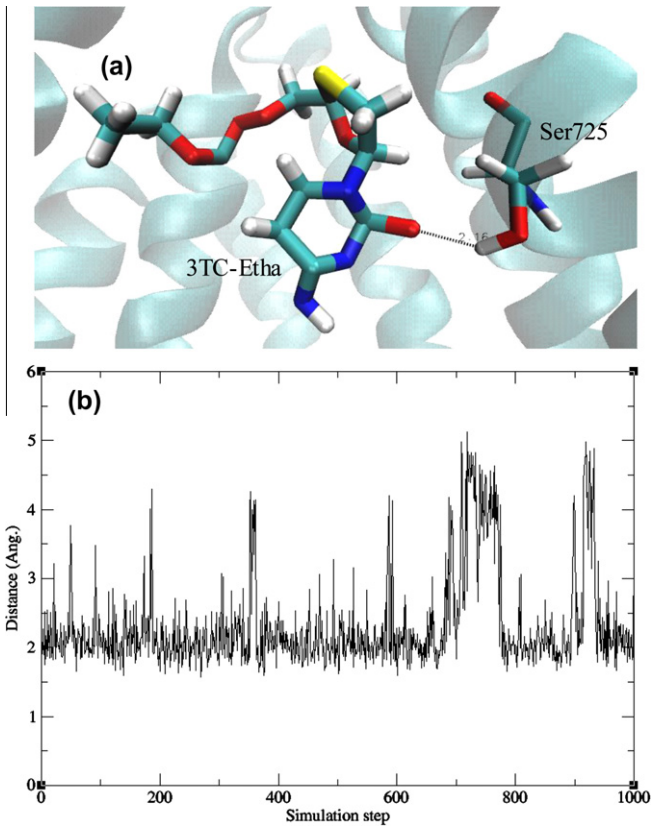

Fig. 14. (a) Hydrogen bond interaction between 3TC-Etha and Ser725, which originated the main stabilizing electrostatic component for the binding of this compound to P-gp. (b) Distance maintained by the hydrogen bond interaction during the molecular dynamics simulation.

pyrimidine ring was located outside the hydrophobic cavity, but several positive (repulsive) electrostatic components were found, particularly for the sidechain of Met68. Based on these observations, it is possible to state that the binding mode of 3TC-Buta was not energetically favored, and thus this compound may not be able to accommodate itself to the binding site cavity and therefore might not be a P-gp substrate. This last remark is in agreement with our permeability studies in the presence of VER (Table 6b).

4. Conclusions

Summing up, we can say that the design of prodrugs of 3TC based on aliphatic alcohol carbonates is a promising strategy to enhance 3TC intestinal permeability, since the enhanced lipophilicity of the resulting derivative confers a higher permeability through the lipid barrier of the intestinal tissue. However, in order to obtain compounds that are able to permeate intact and without the intervention of efflux mechanisms, further structure–stability relationships and molecular modeling studies are needed. Based on the wide variety of aliphatic alcohols available to design new derivatives, some of which have been previously obtained by our research group but whose intestinal permeability has not been studied to date (Ravetti et al., 2009), the possibility of obtaining a prodrug with an adequate stability and low intestinal P-gp efflux seems feasible. Finally, considering the potential intervention of intestinal esterases and cytochrome P450 isoenzymes in the intestinal metabolism of the studied prodrugs, further work regarding the interplay between P-gp and these biotransformation systems is required.

Acknowledgements

The authors gratefully acknowledge financial support from Secretaría de Ciencia y Técnica of the Universidad Nacional de Córdoba (SECYT-UNC), the Ministerio de Ciencia y Tecnología of Córdoba (MINCyT Córdoba), the Consejo Nacional de Investigaciones Científicas y Técnicas (CONICET) and Agencia Nacional de Promoción Científica y Tecnológica (FONCyT) of Argentina. The authors would also like to thank Dr. L. Alassia (FILAXIS Laboratories) for supplying 3TC. María S. Gualdesi acknowledges a fellowship from CONICET, Argentina. Mario A. Quevedo would also like to acknowledge the GPGPU Computing Group and Dr. Nicolás Wolovick from the Facultad de Matemática, Astronomía y Física (FAMAF), Universidad Nacional de Córdoba, Argentina, for providing access to computing resources.

References

Aller, S.G., Yu, J., Ward, A., Weng, Y., Chittaboina, S., Zhuo, R., Harrell, P.M., Trinh, Y.T., Zhang, Q., Urbatsch, I.L., Chang, G., 2009. Structure of P-glycoprotein reveals a molecular basis for poly-specific drug binding. Science 323, 1718–1722.

Allouche, A.R., 2011. Gabedita – a graphical user interface for computational chemistry softwares. J. Comput. Chem. 32, 174–182.

Anastasi, C., Vlieghe, P., Hantz, O., Schorr, O., Pannecouque, C., Witvrouw, M., De Clercq, E., Clayette, P., Dereuddre-Bosquet, N., Dormont, D., Gondois-Rey, F., Hirsch, I., Kraus, J.-L., 2003. Are 5′-O-Carbamate-2′,3′-dideoxythiacytidine new anti-HIV and anti-HBV nucleoside drugs or prodrugs? Bioorg. Med. Chem. Lett. 13, 2459–2463.

Andrew, R.Z., 2010. The evolution of HIV treatment guidelines: current state-of-the-art of ART. Antiviral Res. 85, 241–244.

Balimane, P.V., Chong, S., Morrison, R.A., 2000. Current methodologies used for evaluation of intestinal permeability and absorption. J. Pharmacol. Toxicol. Methods 44, 301–312.

Breedveld, P., Beijnen, J.H., Schellens, J.H.M., 2006. Use of P-glycoprotein and BCRP inhibitors to improve oral bioavailability and CNS penetration of anticancer drugs. Trends Pharmacol. Sci. 27, 17–24.

Case, D.A., Cheatham Iii, T.E., Darden, T., Gohlke, H., Luo, R., Merz Jr., K.M., Onufriev, A., Simmerling, C., Wang, B., Woods, R.J., 2005. The Amber biomolecular simulation programs. J. Comput. Chem. 26, 1668–1688.

Chimalakonda, K.C., Agarwal, H.K., Kumar, A., Parang, K., Mehvar, R., 2007. Synthesis, analysis, in vitro characterization, and in vivo disposition of a lamivudine–dextran conjugate for selective antiviral delivery to the liver. Bioconjug. Chem. 18, 2097–2108.

Cihlar, T., Ray, A.S., 2010. Nucleoside and nucleotide HIV reverse transcriptase inhibitors: 25 years after zidovudine. Antiviral Res. 85, 39–58.

Dahan, A., Amidon, G.L., 2009. Small intestinal efflux mediated by MRP2 and BCRP shifts sulfasalazine intestinal permeability from high to low, enabling its colonic targeting. Am. J. Physiol. Gastrointest. Liver Physiol. 297, G371–G377.

Esté, J.A., Cihlar, T., 2010. Current status and challenges of antiretroviral research and therapy. Antiviral Res. 85, 25–33.

Gagey, D., Ravetti, S., Castro, E.F., Gualdesi, M.S., Briñon, M.C., Campos, R.H., Cavallaro, L.V., 2010. Antiviral activity of 5′-O-carbonate-2′,3′-dideoxy-3′-thiacytidine prodrugs against hepatitis B virus in HepG2 2.2.15 cells. Int. J. Antimicrob. Agents 36, 566–569.

Gao, H.Q., Boyer, P.L., Sarafianos, S.G., Arnold, E., Hughes, S.H., 2000. The role of steric hindrance in 3TC resistance of human immunodeficiency virus type-1 reverse transcriptase. J. Mol. Biol. 300, 403–418.

Hawkins, P.C.D., Skillman, A.G., Warren, G.L., Ellingson, B.A., Stahl, M.T., 2010. Conformer generation with OMEGA: algorithm and validation using high quality structures from the protein databank and cambridge structural database. J. Chem. Inf. Model. 50, 572–584.

Kuhn, B., Gerber, P., Schulz-Gasch, T., Stahl, M., 2005. Validation and use of the MM-PBSA approach for drug discovery. J. Med. Chem. 48, 4040–4048.

Mariappan, T.T., Singh, S., 2007. Gastrointestinal permeability studies using combinations of rifampicin and nucleoside analogue reverse transcriptase inhibitors in rats. Indian J. Med. Res. 39, 284–290.

McGann, M., 2011. FRED pose prediction and virtual screening accuracy. J. Chem. Inf. Model. 51, 578–596.

Milletti, F., Storchi, L., Sforna, G., Cruciani, G., 2007. New and original pK_a prediction method using grid molecular interaction fields. J. Chem. Inf. Model. 47, 2172–2181.

Moroni, G.N., Quevedo, M.A., Ravetti, S., Briñón, M.C., 2002. Lipophilic character of novel amino acid derivatives of zidovudine with anti HIV activity. J. Liq. Chrom. Rel. Technol. 25, 1345–1365.

Quevedo, M.A., Briñón, M.C., 2009. In vitro and in vivo pharmacokinetic characterization of two novel prodrugs of zidovudine. Antiviral Res. 83, 103–111.

Quevedo, M.A., Nieto, L.E., Briñón, M.C., 2011. P-glycoprotein limits the absorption of the anti-HIV drug zidovudine through rat intestinal segments. Eur. J. Pharm. Sci. 43, 151–159.

Ravetti, S., Gualdesi, M.S., Briñón, M.C., 2008. Lipophilicity of 5′-carbonates of lamivudine with antiretroviral activity. Correlation between different methods. J. Liq. Chrom. Rel. Technol. 31, 1014–1032.

Ravetti, S., Gualdesi, M.S., Trinchero-Hernández, J.S., Turk, G., Briñón, M.C., 2009. Synthesis and anti-HIV activity of novel 2′,3′-dideoxy-3′-thiacytidine prodrugs. Bioorg. Med. Chem. 17, 6407–6413.

Robey, R.W., To, K.K.K., Polgar, O., Dohse, M., Fetsch, P., Dean, M., Bates, S.E., 2009. ABCG2: a perspective. Adv. Drug Deliv. Rev. 61, 3–13.

Samuel, B., 2010. The development of antiretroviral therapy and its impact on the HIV-1/AIDS pandemic. Antiviral Res. 85, 1–18.

Shah, V.P., Midha, K.K., Findlay, J.W.A., Hill, H.M., Hulse, J.D., McGilveray, I.J., McKay, G., Miller, K.J., Patnaik, R.N., Powell, M.L., Tonelli, A., Viswanathan, C.T., Yacobi, A., 2000. Bioanalytical method validation – a revisit with a decade of progress. Pharm. Res. 17, 1551–1557.

Shaik, N., Giri, N., Pan, G., Elmquist, W.F., 2007. P-glycoprotein-mediated active efflux of the anti-HIV1 nucleoside abacavir limits cellular accumulation and brain distribution. Drug Metab. Dispos. 35, 2076–2085.

Sharma, P., Chawla, H.P.S., Panchagnula, R., 2002. LC determination of cephalosporins in in vitro rat intestinal sac absorption model. J. Pharm. Biomed. Anal. 27, 39–50.

Strauch, S., Jantratid, E., Dressman, J.B., Junginger, H.E., Kopp, S., Midha, K.K., Shah, V.P., Stavchansky, S., Barends, D.M., 2011. Biowaiver monographs for immediate release solid oral dosage forms: lamivudine. J. Pharm. Sci. 100, 2054–2063.

Szakacs, G., Varadi, A., Ozvegy-Laczka, C., Sarkadi, B., 2008. The role of ABC transporters in drug absorption, distribution, metabolism, excretion and toxicity (ADME-Tox). Drug Discov. Today 13, 379–393.

Trevor, H., 2010. Understanding and managing the adverse effects of antiretroviral therapy. Antiviral Res. 85, 201–209.

Wallace, A.C., Laskowski, R.A., Thornton, J.M., 1995. LIGPLOT: a program to generate schematic diagrams of protein–ligand interactions. Protein Eng. 8, 127–134.

Zhong, Y., Dai, Z., Xu, Y., Teng, Y., Wu, B., 2012. Synthesis, stability and pharmacological evaluation of a novel codrug consisting of lamivudine and ursolic acid. Eur. J. Pharm. Sci. 45, 110–115.

Zhou, S.F., 2008. Structure, function and regulation of P-glycoprotein and its clinical relevance in drug disposition. Xenobiotica 38, 802–832.